Available online at www.sciencedirect.com

jmr&t Journal of Materials Research and Technology

journal homepage: www.elsevier.com/locate/jmrt

Original Article

Bio-inspired mechanically robust superhydrophobic polypropylene surfaces embedded with silicon carbide whiskers for enhancing bactericidal performance

Jindi Lai [a,c], *Anfu Chen* [a,c,*], *Jing Li* [a], *Yameng Pei* [a], *Seyed Ataollah Naghavi* [c], *Caihong Lei* [a], *Chaozong Liu* [c,**], *Lijia Huang* [b,***]

[a] *Guangdong Provincial Key Laboratory of Functional Soft Condensed Matter, School of Materials and Energy, Guangdong University of Technology, Guangzhou 510006, PR China*

[b] *Department of Operative Dentistry and Endodontics, Guanghua School of Stomatology, Hospital of Stomatology, Sun Yat-Sen University, Guangdong Provincial Key Laboratory of Stomatology, Guangzhou 510000, PR China*

[c] *Institute of Orthopaedics and Musculoskeletal Science, Division of Surgery and Interventional Science, University College London, Royal National Orthopaedic Hospital, London HA4 4LP, United Kingdom*

ARTICLE INFO

Article history:
Received 24 November 2022
Accepted 10 January 2023
Available online 18 January 2023

Keywords:
Superhydrophobic surfaces
Hierarchical structure
Mechanical robustness
Antibacterial activity
Compression molding

ABSTRACT

The risk of spread of antibiotic-resistant bacteria leads to the growth of implant-associated infection, necessitating the large-scale fabrication of antibacterial materials. The successfully synthetic superhydrophobic and bactericidal materials without durable surfaces are easy to destroy and so difficult to use in a large-scale production in terms of manufacturing costs in performing experiments and processes. In this work, two kinds of microfeatured sieves dipped with high length-diameter ratio silicon carbide whiskers (SiCw) are used as templates for the fabrication of micropillared polypropylene (PP) surfaces embedded with nanospiked SiCw exposed in different postures of standing via a simple low-cost micro-compression molding method. The standing SiCw nanospikes endow the micropillared PP surfaces with a high contact angle (CA) of 153.9° decreased by less than 8° after a wear distance of 1500 mm, exhibiting robust antiwetting and antifriction properties. Further, the nanospiked micropillared PP surfaces exhibit extremely low adhesion and moderate antibacterial efficacy. The micro-/nanoconstructed PP surfaces is expected to approach towards large-scale industrial production for biomedical applications.

* Corresponding author.
** Corresponding author.
*** Corresponding author.
E-mail addresses: anfuchen@gdut.edu.cn (A. Chen), chaozong.liu@ucl.ac.uk (C. Liu), huanglj35@mail.sysu.edu.cn (L. Huang).

https://doi.org/10.1016/j.jmrt.2023.01.069

1. Introduction

Plants and animals in nature have functional characteristics that serve to jealously protect themselves against living creatures higher up on the food chain in their natural habitat, access, and retain resources [1]. Obviously, this is key to successful survival, growth, and reproduction [2,3]. As distinctive structures derived from leaf tissue of plants, spines protect the plant families from being consumed excessively by herbivores [4]. Just as the acacia trees with unique fern-like leaves featuring regular spikes defend themselves against giraffes to a certain extent. The biological power of microtextured lotus leaves and nanotextured cicada wing surfaces on bacteria has attracted much attention [5–7]. The regular spiked nanoarchitectures on the dragonfly and the cicada wing surfaces can penetrate deep into the bacterial cell wall, then stretch it, and finally lead to mechanical rupture of bacterial cells. Moreover, this antibacterial process is achieved by physical stretching and damage, instead of by chemical fungicides [8,9]. Inspired by this defense mechanism of the spiked structures, the bacterial adhesion to solid surfaces at micro scale may be further undermined by constructing nanospikes on superhydrophobic microstructured polymer surfaces. Thus, this effectively ameliorates the antibacterial effect.

Furthermore, by mimicking the micromorphologies and physicochemical properties of these plant and animal surfaces, artificial superhydrophobic polymers with excellent properties in self-cleaning [10], anti-icing [11], anti-fogging [12], anti-corrosion [13], and anti-bioadhesion [14] are fabricated and applied in various fields of microfluidic [15], droplet transportation [16], desalination [17], optical devices [18], green printing [19], oil-water separation [20], sensors [21], and anti-bacteria [22]. It is well known that bacterial infection of biomaterials is the most important cause of surgical failure and a major problem in clinical medicine. Today, antibiotics are used as the mainstream treatment to suppress bacterial infections, but overuse of antibiotics leads to bacterial resistance. Undoubtedly, this is detrimental to both postoperative recovery and, worse, leads to increased infection and consequently death of the patient. In recent years, antimicrobial strategies that micro-/nanoarchitecture is constructed on polymer surfaces have received widespread attention. The micro-/nanoarchitecture would not cause resistance to antibiotic drugs, and they rely on a safe, efficient, and direct antimicrobial method by reducing bacterial adhesion to block subsequent biofilm formation and proliferation of bacteria; currently, there are three main types of such antimicrobial surfaces: antiadhesion-based, release-based, and contact-based antimicrobial polymer surfaces [23]. Linklater et al. demonstrated that the adsorption of bacteria on the surface of the nanopillar exposes the cell membrane to increasing pressure and the cell membrane is stretched beyond its elastic limit, resulting in rupture of the membrane [24]. Lin et al. demonstrated that nanomorphologies (e.g., nanopillars, nanostructures, and nanocones) based on physical structures rather than chemical biocides can show equally effective and high bactericidal activity without leading to antibiotics resistance [25]. Radically different from the conventional dilemma about bacterial resistance to antibiotics, the fact that antibacterial polymer surfaces were modified with micro-/nanostructures is obviously a more effective defense strategy to undermine bacterial adhesion as well as antibiotic-induced biofilm formation. Also, this defense strategy raises resistance to implant-associated infection. More specifically, the weakened bacterial adhesion benefits from the significantly enhanced antiwetting properties, i.e., superhydrophobicity.

Generally, these superhydrophobic surfaces are determined by micro-/nanostructure and low-surface-energy substances. The air pockets forming between water droplets and the micro-/nanostructured surfaces leave the droplet to suspend on rough surfaces. With the progress of society, superhydrophobic surfaces have shown great potential for application in a variety of fields in industrial and academic research [26,27]. However, micro-/nanostructures constructed on polymer surfaces are susceptible to mechanical damage, so it is difficult to maintain the superhydrophobic surface for a long life [28]. Wang et al. reported that researchers had prepared a series of superhydrophobic materials by designing reasonable structures, building chemical bonds, strengthening the interface between hydrophobic matter and substrates [29]. These superhydrophobic surfaces endowed with self-healing properties obtained a prolonged service life. In practical applications, however, the collapse of micro-/nanostructures induces irreversible damage to superhydrophobicity. More notably, the abovementioned methods are liable to be subjected to the low interfacial strength of particles and low compatibility with the polymer matrix. Therefore, the fact that the low mechanical durability for polymer poses a threat to wetting stability of superhydrophobic surfaces limits their large-scale applications. Therefore, the durability of superhydrophobic polymers is a key performance indicator for their application [30,31]. Especially in the field of biomaterials, the stability of the micro-/nanostructure is directly related to the antimicrobial performance. Therefore, researchers have introduced high performance silicon carbide materials into micro-/nanostructured surfaces to enhance the mechanical strength of the surface structure, promote the biocompatibility of the material surface, and enhance the antimicrobial properties of the surface [32]. However, the efficacy of the carbon material to the mechanical strength of the micro-nano structure is limited. Without regard to the durability, Roy et al. fabricated bactericidal allosteric nanostructures by dry etching and obtained efficient anti-bacterial properties [33]. Sandra et al. used low-energy ion beam irradiation techniques to fabricate bioinspired nanostructures in bacterial cellulose hydrogels featuring resistance to water immersion. The nanostructures were able to penetrate cells and cause cell damage, demonstrating the ability to endow a hydrogel with bactericidal properties by just tailoring surface textures on a nanoscale [34]. However, the preparation processes of these superhydrophobic surfaces are highly cost-intensive and unnecessarily complicated (e.g., the required harsh chemical conditions and the corresponding equipment). Obviously, it is urgent to propose a simple and effective method for the fabrication of durable superhydrophobic antibacterial polymers in terms of nanospiked micropillars on surfaces.

Natural superhydrophobic surfaces can properly maintain antiwetting properties through metabolic pathways or low-surface-energy secretions, while artificial superhydrophobic

surfaces cannot spontaneously heal or reconstruct damaged structures in most cases. The fact that the structural integrity of surface is difficult to preserve leads to the loss of superhydrophobic properties after abrasion exposure in practical applications [35–39]. As one of the most commonly used general-purpose plastics, polypropylene (PP) resin has unique advantages of low surface energy, good thermal processing performance, and high mechanical strength. Also, silicon carbide whiskers (SiCw) have the characteristics of high hardness, high strength, and heat resistance. In this work, applying the micro-compression molding technique, a simple and effective method was proposed to fabricate durable superhydrophobic polymer surfaces via embedding the SiCw into the surface layer of micropillared PP substrates as ideal fractal spiked nanostructures. The SiCw with different concentrations in alcohol suspensions were dipping into the sieves as templates and then were transferred onto to micropillared PP substrates, forming superhydrophobic SiCw-covered micropillared PP surfaces, i.e., nanospiked micropillared PP surfaces. Further, the antiwetting and antibacterial properties were investigated. Without any chemical biocides, the nanospiked micropillared PP surfaces take a decisive antibacterial action to prevent bacterial fast growth and mass reproduction.

2. Experimental section

2.1. Materials

The polymer used as received in this work was commercial PP (grade CJS700, Sinopec Corp. Guangzhou, China) with a melt flow index of 11.0 g/10 min (230 °C, 2.16 kg). The high-length-diameter ratio SiCw with a diameter of 5–10 nm and a length of 1–3 μm were provided by Yangzhou Tingyue Technology Co., Ltd. The 2.5% glutaraldehyde was purchased from Aladdin, China. Phosphate buffered saline (PBS, pH = 7.4, c = 1 × , Thermo Fisher Scientific). The 500-mesh and 3000-mesh sieves serve as templates with a cut size of 25 × 25 mm^2.

2.2. Dipping pretreatment of templates

Firstly, the weighed SiCw were dispersed in the anhydrous ethanol, and the SiCw/ethanol suspension was given a 300 W (40 kHz) ultrasonic treatment for 2 h to ensure that the SiCw were evenly dispersed in the ethanol, instead of agglomerates. Secondly, the ultrasonic cleaning treatment for the tailored 500-mesh and 3000-mesh sieves in the anhydrous ethanol solvent for 15 min, ensuring the removal of the stains as well as fine dust on their surfaces. Five drops of the SiCw/ethanol suspension with the specific concentration were uniformly placed on the sieves using a disposable rubber-tipped dropper. Sieves coated with uniformly distributed SiCw are obtained by evaporation under ambient conditions.

2.3. Preparation of micropillared PP surfaces

The SiCw-treated 500-mesh and 3000-mesh sieves were used as templates to prepare micropillared PP surfaces by the micro-compression molding technique, as shown in Fig. 1a. The experiment was performed at a mold temperature of 180 °C, compression pressure of 5 MPa, and pressure-holding time of 3 min. The sieve templates were coated with SiCw concentrations of 0, 5, 10, 15, 20, 25, and 30 mg/mL (marked as S1 to S7), respectively. For PP surfaces with nanospiked micropillars molded with 500-mesh sieves, the corresponding samples prepared under the abovementioned process are referred to as 5S1 to 5S7; for PP surfaces with nanospiked micropillars molded with 3000-mesh sieves, the corresponding samples are referred to as 3S1 to 3S7.

2.4. Wear test

Superhydrophobic state may be created by the formation of new asperities on the solid surface caused by lower grit coarse sandpaper (280–400#). In contrast, the higher grit polished sandpaper undermines the superhydrophobic properties by removing the asperities on the solid surface [40]. Therefore, the abrasion resistance of nanospiked micropillared PP surfaces was investigated under slide travels with a constant velocity on 2000 grit sandpaper, and the schematic diagram of the test process was shown in Fig. 1b. The samples fixed to glass slides were subjected to a weight of 200 g, and the other side of the sample surface possessing micro-/nanoarchitectures directly contacted with the sandpaper and slid forward on it using a modified universal testing machine as equipment for the precise control of a constant moving speed and 500-, 1000-, and 1500-mm friction distances [41].

2.5. Characterization of micromorphologies and wettabilities

Two field emission scanning electron microscopes (SEM, Hitachi SU8010 and S-4800, Hitachi Ltd., Tokyo, Japan) were used to characterize the surface micromorphology of nanospiked micropillared PP surfaces and surface-associated bacteria, respectively. Samples with bacteria were subjected to SEM observation as described before [42]. Briefly, samples were rinsed twice with the sterile PBS and fixed with 2.5% glutaraldehyde at 4 °C overnight, followed by serially dehydrated using the gradient ethanol (50%, 70%, 85%, 90%, and 100%) for 10 min each. Prior to the SEM, the samples were freeze-dried overnight, coated with platinum by ion sputtering, and observed in high vacuum state mode at an accelerating voltage of 5 kV. A fully automatic contact angle measuring and contour analysis system (OCA 100, Dataphysics Instruments GmbH, Filderstadt, Germany) was used to measure the water contact angle (CA) of each sample before and after each friction cycle. Here, the test droplet used for the CA measurement was set at 4 μL. A 500 frame per second high-speed CCD camera (TS, Fastec Imaging, San Diego, CA, USA) was used to record droplet impact experiments, and the nanospiked micropillared PP surfaces were provided with lighting by two cold light sources. A surface tension apparatus (DCAT21, DataPhysics Instruments GmbH, Filderstadt, Germany) was used to test the surface adhesion force of the samples before and after wear.

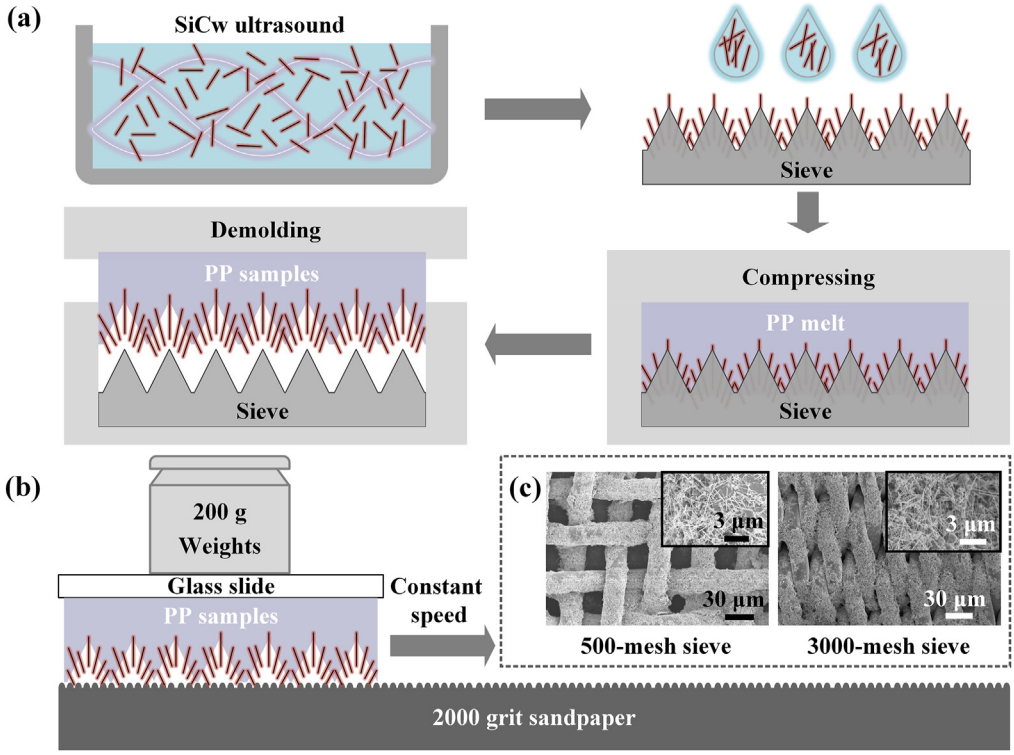

Fig. 1 – Schematics of (a) SiCw dipping pretreatment of sieve templates, process of micro-compression molding of nanospiked micropillared PP surfaces, and (b) frictional wear experiment; (c) SEM images of SiCw-coated sieves with SiCw concentration of 20 mg/mL.

2.6. *Colony forming unit counting*

Incubation of the bacterial cultures was performed on nanospiked micropillared PP surfaces using *Candida albicans* (*C. albicans*) with a size of 4–6 μm to count colony forming unit (CFU). The *C. albicans* ATCC 10231 was stored in 15% (vol/vol) glycerol stock at −80 °C and maintained on yeast extract-peptone-dextrose medium (YPD, Macklin, China) plus uridine (1% yeast extract, 2% peptone, 2% dextrose, and 80 μg/mL uridine) prior to experiments. Cultures were propagated overnight in YPD medium with uridine at 30 °C on an orbital shaker at 200 rpm. Overnight cultures were grown in YPD and uridine broth at 30 °C for 16~18 h and then diluted to a concentration of 1×10^5 CFU mL^{-1} for further studies.

The antiadhesive property of samples was assessed by a colony forming assay gauging the number of bacteria attached on the surface. To be specific, the prepared samples were placed onto the bottom of 12-well plate and then *C. albicans* suspension (2 mL, 1×10^5 CFU mL^{-1}) was pipetted into the wells, followed by incubation at 30 °C for 24 h. After the incubation was terminated, the samples were removed carefully and rinsed with the sterile PBS twice to remove unbound bacteria. Then samples were transferred to a new sterile 12-well plate with 1 mL PBS in each well, following ultrasonic for 10 min with 40% power to dislodge the attached bacteria. Finally, bacterial amount was determined using a serial dilution plating assay. Briefly, bacterial suspension was serially diluted and spread on YPD agar plate and further incubated at 30 °C overnight. Tests were repeated three times for each group and the antibacterial efficiency is obtained by the following equation:

$$\text{Antimicrobial efficiency } (\%) = \left[\frac{(A-B)}{A}\right] \times 100 \quad (1)$$

where A and B are the average viable CFU/mL on the control group (pure flat PP surface) and the experimental group, respectively.

2.7. *Fluorescence (Live/Dead) staining*

Bacterial viability tests were performed using fluorescence microscopy. The harvested samples were rinsed with sterile saline twice and placed in a new 12-well plate. Two fluorescent nucleic acid dyes, 4',6-diamidino-2-phenylindole (DAPI, 98%, Aladdin, China) and propidium iodide (PI, 98%, Aladdin, China), were employed to stain *C. albicans* as reported before [43]. More specifically, 0.5 mL DAPI and PI dye from the Live/Dead Viability Kit (Invitrogen) were added onto the sample and incubated at 30 °C for 15 min in the dark. Then the samples were rinsed with sterile saline gently and observed by laser scanning confocal microscope (Olympus FV3000, Tokyo, Japan). The excitation for live bacteria (indicating green fluorescence) and dead bacteria (indicating red fluorescence) were demonstrated with two wavelengths at 488 and 561 nm, respectively.

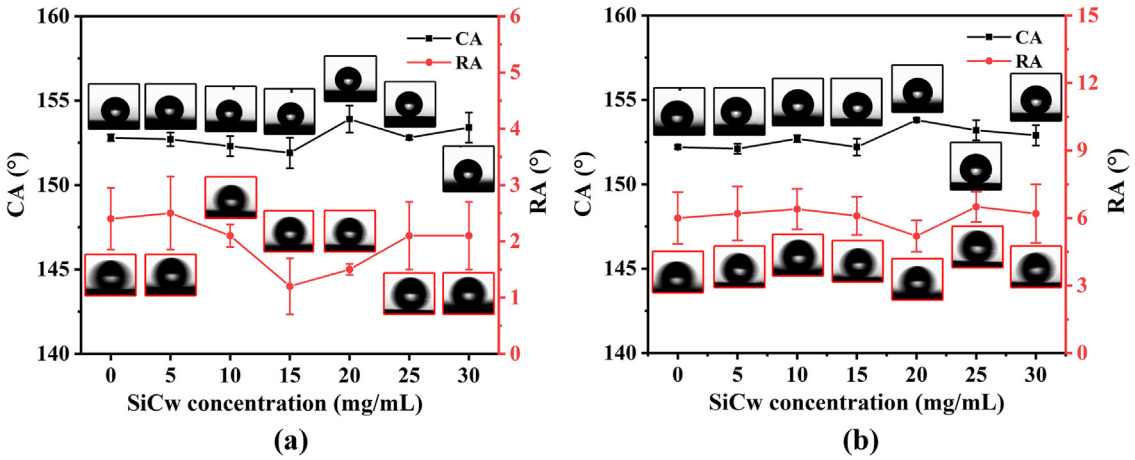

Fig. 2 – Wetting states of nanospiked micropillared PP surfaces molded with (a) 3000- and (b) 500-mesh sieves dipped with different SiCw concentrations.

3. Results and discussion

3.1. *Optimization of SiCw concentrations*

To tune the SiCw content, the wettabilities of the PP replicas coated with different SiCw concentrations were compared, and their CA values as well as optical images are shown in Fig. 2. According to CA tests, all the nanospiked micropillared PP surfaces achieved superhydrophobicity. Compared to the micropillared PP surface molded without the SiCw-coated sieve (CAs of 152.2°–152.8°), there is no significant fluctuation in the CA values is for the PP replicas molded with sieves coated with SiCw concentrations of below 15 mg/mL, and the CA increases to 153.8°~153.9° for the one with SiCw concentrations of 20 mg/mL. When the SiCw concentrations exceed 20 mg/mL, the CAs decrease with different degrees. This may be because the microcavities were blocked by the superfluous SiCw. Obviously, the concentration of 20 mg/mL is selected as the optimized SiCw concentration for the fabrication of the nanospiked micropillared PP surfaces.

3.2. *Distribution of SiCw on micropillared PP surfaces*

To explicitly demonstrate the topography of microstructured PP surfaces coated with different SiCw concentrations, their SEM images were shown in Fig. 3. As can be seen, the pyramid-shaped and cube-shaped micropillars as well as ridge-like

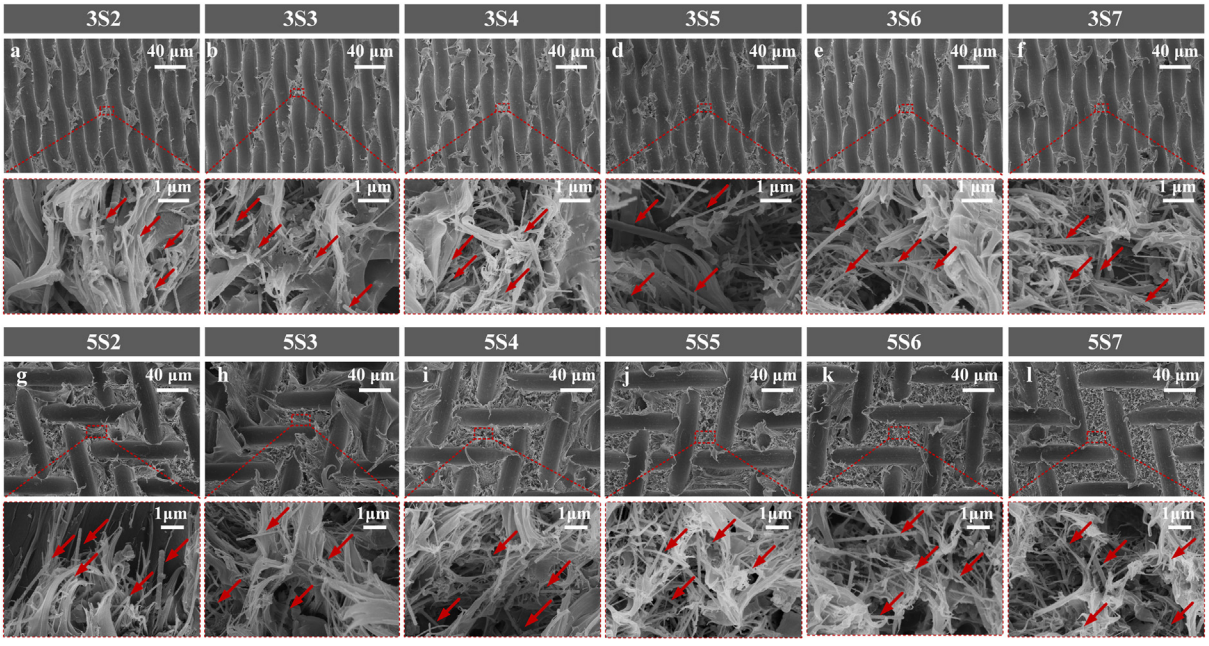

Fig. 3 – SiCw distributed on micropillared PP surfaces molded with (a–f) 3000-mesh and (g–l) 500-mesh sieves coated with SiCw concentrations ranging from 5 to 30 mg/mL.

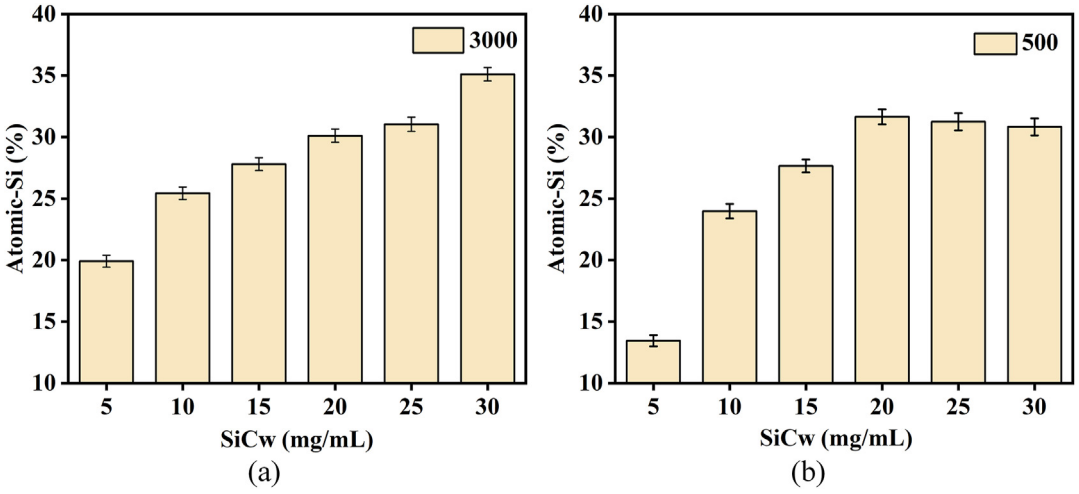

Fig. 4 – Atomic-Si concentration on nanospiked microstructured PP surfaces molded with (a) 3000- and (b) 500-mesh sieves in terms of Atomic-Si distributed in EDS images as a function of SiCw concentration.

structures are duplicated from the 3000-mesh and 500-mesh sieves coated with different SiCw contents, respectively. Besides, villi as submicron structure appear on the micropillars after detaching from the sieves. These three kinds of structures act as dual-scale submicron-/microstructures, which fortunately remain undamaged after demolding. Most importantly, the results evidenced that the SiCw were successfully transferred from the SiCw-coated sieves onto the micropillared PP surfaces. Obviously, the SiCw serving as spiked nanoarchitectures cover micropillared PP surfaces and shape hierarchical micro-/nanostructures. As shown in magnified SEM images and data statistics as estimated from EDS images (Fig. S1 Supplementary Information) in Figs. 3 and 4, the nanospikes distributed mainly in the micropillars and the ridge-like structures are clustered together and grow ever denser with the SiCw concentration. More specifically, a small segment of the high-length-diameter ratio SiCw is embedded into the layer of PP surfaces, and the rest part of the SiCw is completely exposed in different postures of standing. The nanospiked micropillared PP surfaces (3S7 and 5S5) molded with the sieves coated with 30 and 20 mg/mL SiCw do possess the maximum SiCw, respectively. Combining with the CA results in Fig. 2, the maximum SiCw distribution and the maximum CA show inconsistency for the samples molded with the 3000-mesh sieves, while the maximum SiCw distribution and the maximum CA show consistency for the samples molded with the 500-mesh sieves. This may be because the blocking of the microcavity in 3000-mesh sieves hinders the formation of well-developed micropillars with above 20 mg/mL SiCw. To see more clearly, the SEM images of the 3S2, 3S5, 5S2, and 5S5 samples tilted at an angle of 45° are provided in Fig. S2 (Supplementary Information).

Fig. 5 shows XRD diffractograms for the SiCw and the sieves coated with and without SiCw. The characteristic diffraction peaks of SiCw before and after coating the sieves all appear at 36.0°,41.4°,60.0°,71.7°,75.6°, which are in perfect agreement with the diffraction peaks of the standard PDF of the cubic crystal system (zinc-blend (cubic)) 3C–SiC (β-SiC, JCPDS Card No.29-1129). In the plots of SiCw before and after coating, the SF peak exists at 33.6°, indicating that the stacking faults may exist during the process of whisker generation. Stacking faults can change the crystal structure and generate a large number of dislocations and vacancies [44]. Also, the inconspicuous diffraction peaks of SiCw at the same position ranging from 36.0°, 41.4°, 60.0°, 71.7°–75.6° can be observed on the curves for the 500-mesh and the 3000-mesh sieves coated with SiCw. The fact that the diffraction peaks of SiCw seem weak is probably due to the high intensity of the stainless-steel sieves at the diffraction angle. As expected, the SiCw are successfully transferred from the sieves onto the PP surfaces, and the corresponding XRD diffractograms of nanospiked micropillared PP replicas are shown in Fig. S3 (Supplementary Information).

Compared with the SEM images of SiCw-coated sieves in Fig. S4 (Supplementary Information), the SiCw seem evenly distributed in both sieves coated with 20 mg/mL SiCw without

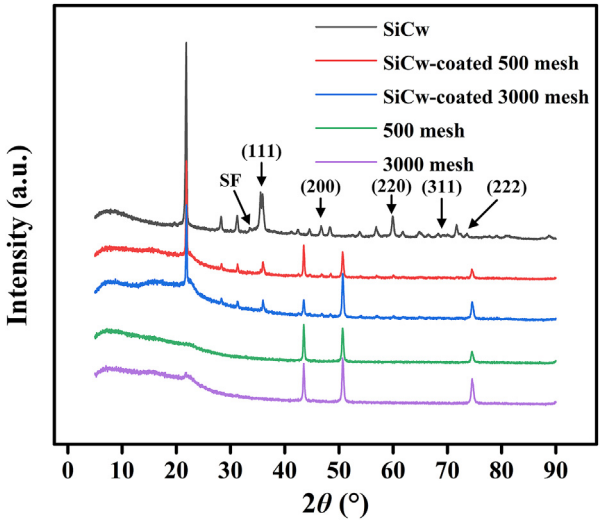

Fig. 5 – XRD diffractograms of the SiCw and 500-mesh and 3000-mesh sieves coated with and without SiCw.

blocking the holes. For a reduced distribution of SiCw on the micropillared PP surface molded by sieves coated with SiCw of above 20 mg/mL, it is indeed attributed to the blocking of microcavities, which is relative to the pore size of sieves. Because the aperture of 500-mesh sieve is much larger than that of 3000-mesh sieve (Fig. 1c), the superfluous SiCw slip away through these pores. Moreover, the SiCw originally adhered to the sieve will run off due to the fluidity of the dispersing agent. In comparison, the SiCw cannot easily run off the 3000-mesh sieve with much smaller pores, and so more SiCw get sticking to the sieve. This indicates that the distribution of SiCw on the nanospiked micropillared PP surfaces can be controlled by tuning SiCw concentration gradients to the maximum concentration (Fig. 4b). This can be inferred from the comparison of laser confocal images, as shown in Fig. S5 (Supplementary Information).

3.3. *Wettabilities and micromorphologies of abraded nanospiked micropillared PP surfaces*

Low resistance to wear is identified as a significant bottleneck-induced limitation in the application of superhydrophobic polymers. Currently, the most commonly used way to assess the wear resistance of superhydrophobic polymers is abrading on sandpaper, providing a preliminary determination of the lifetime of superhydrophobic materials [45]. Since the SiCw distribution on the micropillared PP surfaces changes with the SiCw concentration, different SiCw concentration gradients may have an impact on the friction and wear performance of the nanospiked micropillared PP surfaces. To determine whether the nanospiked micropillars on PP surface could maintain surface wettabilities after a certain distance of abrasion, Fig. 6 shows the CAs of nanospiked micropillared PP surfaces molded with 3000- and 500-mesh sieves as a function of SiCw concentrations after frictional wear at 500-, 1000-, and 1500-mm distances. As can be seen, for replicas duplicated from 3000- and 500-mesh sieves, respectively, the uncoated micropillared PP surface shows a precipitous drop in the CA after a certain distance of wear cycles. It is fortunate that the CAs of nanospiked micropillared PP surfaces molded with 3000- and 500-mesh templates can maintain at above 140° and 145° (even close to 150°), respectively, after the whole wear cycle experiments. The Cassie–Baxter model combined with the contact line density can be used to demonstrate the change of wettabilities of the PP sample surface during the friction test [46]. The increase in CA after abrasion indicates that the solid–liquid contact area fraction increases with the distance of friction. Such a phenomenon would have been a startling departure from tradition that abrasion leads to a decrease in hydrophobicity of solid surfaces [47]. Apparently, the nanospiked micropillared PP surfaces have better wear resistance compared with the uncoated micropillared PP surface. As the SiCw concentration increases, the CA of the samples after a wear distance of 1500 mm also gradually increases, indicating that the SiCw can maintain a better hydrophobic performance of the samples from another perspective. For the nanospiked micropillared PP surfaces molded with the 3000-mesh sieve (Fig. 6a), the sample coated with SiCw of 30 mg/mL just shows a tiny increase in CA than the one coated with SiCw of 20 mg/mL after abrasion. This indicates that the SiCw content of 20 mg/mL is optimized and enough for obtaining considerable resistance to wear. From the standpoint of large-scale applications, it would be more economical to use the SiCw content of 20 mg/mL to treat the sieves for surface microstructures. For the nanospiked micropillared PP surfaces molded with the 500-mesh sieve (Fig. 6b), the samples coated with 20 mg/mL SiCw maintain the highest CA after a wear distance of 1500 mm, exhibiting a higher wear resistance and hydrophobic effect. Further, the micropillared PP surfaces molded with sieves coated with SiCw of 20 mg/mL can maintain high CAs after a certain wear cycle. It can be concluded that altering the SiCw concentration can vary CA of the nanospiked micropillared PP surface after the wear cycle, and the CA can maintain to the maximum within the suitable concentration range. This indicates that the SiCw embedded in the surface layer of samples can improve the wear resistance of micropillared PP surfaces.

The results of the abrasion test are relative to the distribution of SiCw with different concentrations, echoing the optimized selection for the SiCw content of 20 mg/mL

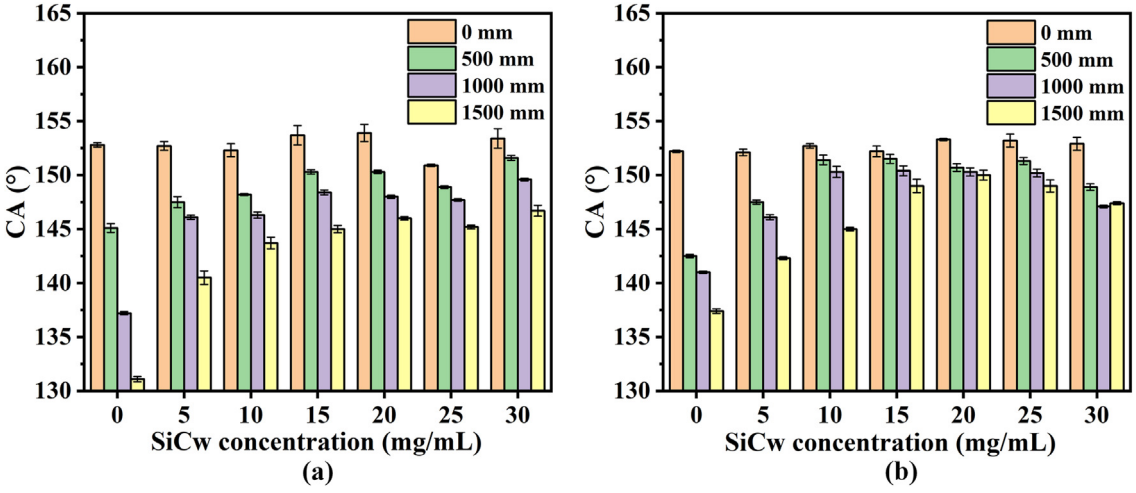

Fig. 6 – Contact angles of nanospiked micropillared PP surfaces molded with (a) 3000- and (b) 500-mesh sieves as a function of SiCw concentrations after frictional wear at 500-, 1000-, and 1500-mm distances.

mentioned above. To further observe and analyze their morphology, Fig. 7 shows SEM images of abraded micropillared PP surface molded with sieves coated without and with SiCw. Also, the SEM images of the abraded flat PP surface was provided in Fig. S7 (Supplementary Information). As can be seen, the abraded micropillared PP sample without SiCw coating undergone a 1500 mm wear distance, on which the micropillars are severely damaged. Especially, the surface morphology of micropillared PP samples molded with 3000-mesh sieve is close to that of flat PP samples Fig. S7d). In consideration of their CAs decreased by 20° and shifted from 150° to 130° (Fig. 6). Therefore, the structural damage is the major reason for the PP samples losing their superhydrophobic properties during the friction process.

For the micropillared PP samples molded with sieves coated with 5 and 20 mg/mL SiCw, respectively, minor wear is seen as an essential credential for achieving highly hydrophobic after a certain distance of abrasion. More specifically, compared to the micropillared PP sample coated with 5 mg/mL SiCw, the one with 20 mg/mL SiCw has less structural wear, and its structural integrity of surface is higher. Moreover, the samples molded with the 500-mesh sieve can maintain a better structural integrity of the surface when suffering from severe damage compared with the samples molded with the 3000-mesh sieve with 20 mg/mL. Also, the vast majority of the SiCw can maintain standing state for the micropillared PP surfaces molded by the 3000-mesh sieve coated with SiCw content of above 15 mg/mL; while the vast majority of the SiCw achieves standing state for the micropillared PP surfaces molded by the 500-mesh sieve coated with SiCw content of above 20 mg/mL. This can be attributed to the fact that the size of micropillars on the sample molded with the 500-mesh sieve is larger than the one molded with the 3000-mesh sieve due to the larger pore size of 500-mesh sieve covered with more SiCw. Moreover, the pyramid-shaped micropillars on the PP surfaces molded with 3000-mesh sieves are more likely to keep the SiCw standing, forming nanospiked micropillars. To achieve the nanospiked micropillars with standing state for the cube-shaped micropillars on the PP surfaces molded with 500-mesh sieves, the SiCw content of above 20 mg/mL is required due to a larger specific surface area. The micropillars constructed on the PP surface molded via the 500-mesh sieve with larger pore size is thick and strong, while the micropillars constructed on the one molded via the 3000-mesh sieve with smaller pore size is thin and weak. The thinner the micropillar constructed on the PP surface is, the more susceptible it is to mechanical damage. When an external load acts on the micropillared PP surfaces,

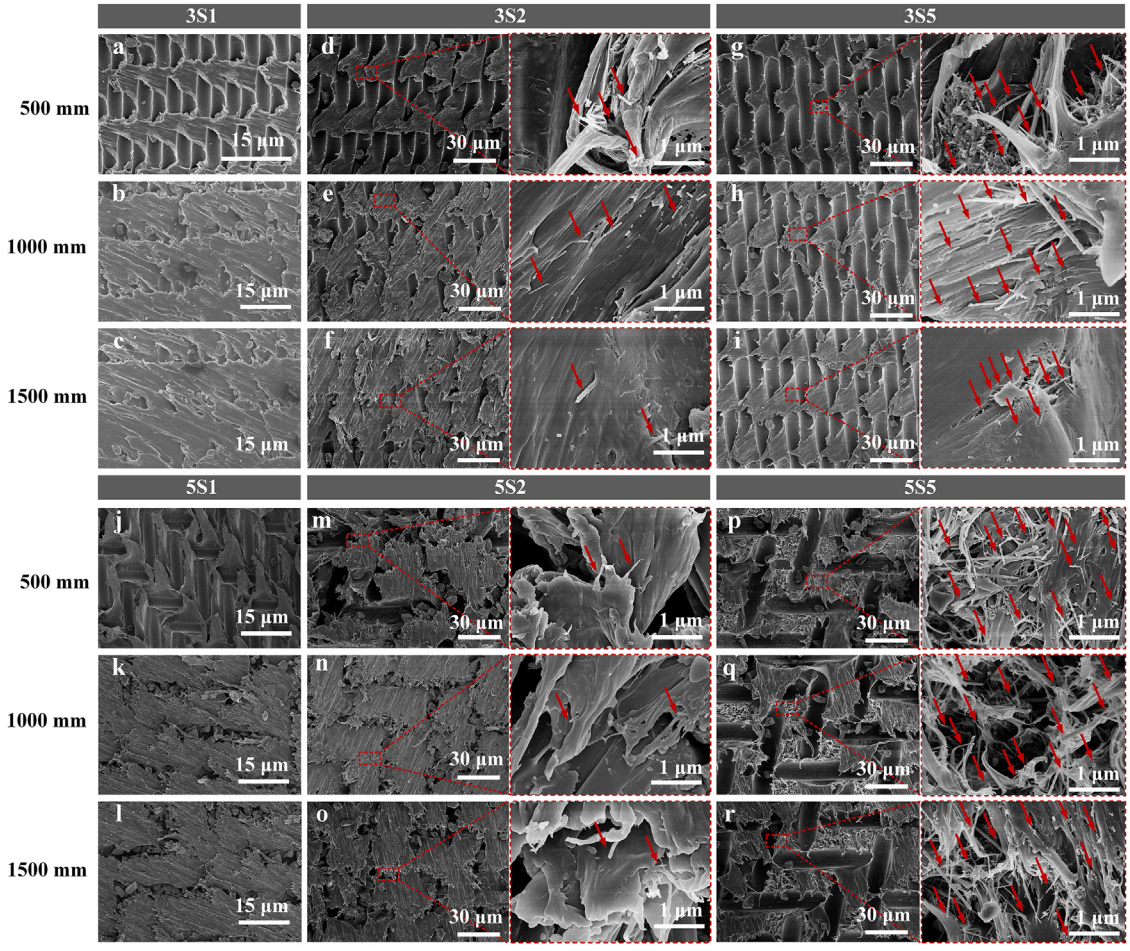

Fig. 7 – SEM images of abraded nanospiked micropillared PP surfaces molded with (a–i) 3000-mesh and (j–r) 500-mesh sieves coated without and with SiCw contents of 5 and 20 mg/mL.

the elastic deformation of the standing SiCw can dissipate a large amount of energy from the external load. This protects the micropillar itself and the nanoscale nanospiked structure on the surface. More importantly, the SiCw are embedded in the surface layer and cannot fall off the surface with ease. Therefore, a squat structure is an essential prerequisite for the excellent wear resistance and durability, and large specific surface area can retain more SiCw covering the surface layer. From a certain point of view, the standing SiCw endow the micropillared PP surfaces with strong resistance to wear and substantially contribute to the maintaining of the highly superhydrophobic state after a certain distance of friction.

3.4. *Droplet impact on nanospiked micropillared PP surfaces before and after wear*

Droplet impact experiments are commonly used to evaluate the wetting stability of superhydrophobic surfaces [48,49]. The impact processes were carried out at room temperature and recorded, as shown in the Video S1–S4 (Supplementary Information). Diagram of droplet impact on unabraded surface is shown in Fig. S8 (Supplementary Information). Fig. 8 shows typical images of abraded micropillared PP surfaces molded with 3000- and 500-mesh sieves coated with 20 and 5 mg/mL SiCw, respectively. The 7 μL droplets are impacting on the four selected micropillared PP surfaces at a velocity of 1 m s^{-1}. Since the droplets are subjected to the surface adhesion force after impacting the micropillared surfaces, some of the kinetic energy of the droplets dissipate during this impact process. The remaining kinetic energy is calculated from the gravitational potential energy at the highest position, where the droplet rebounds. Then, the impact resistance of the micropillared PP surfaces can be evaluated through the rebound height. The dynamic process of droplet impacting on abraded micropillared PP surfaces can be divided into four dynamic behaviors: spreading, retracting, rebounding, and fragmenting. After droplets impacts on the sample surface, they withdraw from an expanded state and is in an unsteady state during the retraction phase. The lower end of the droplet on the sample surface is stretched under the action of surface tension. As the rebound phase comes, the droplet forms a narrow upper and wide lower shape, and then becomes a wide upper and narrow lower shape. At this time, a large part of the kinetic energy of the droplet is converted into the gravitational potential energy, presenting in the form of the maximum height that the droplet can reach. At the first several times, the droplet still has enough surface tension and inertial force to break away the sample surface. Because the sample surface has the adhesion to the droplet, however, the kinetic energy of the droplet at the lower end needs to overcome not only the gravitational potential energy but also the surface adhesion to break away the sample surface. At last, the kinetic energy of the lower droplet is not enough to overcome the sample surface adhesion force. The upper droplet keeps moving upward and oscillating until its kinetic energy is completely exhausted. Then, the upper droplet falls back to the sample surface. As time passes, the droplet finally comes to rest on the sample surface.

Based on the comparison of the height of the rebound, the adhesion of the abraded 5S5 surface to the droplet is less than that of abraded 5S2 surface. As shown in Fig. 9, the surface adhesion of the abraded 3S5 and 5S5 samples is always lower than that of the abraded 3S2 and 5S2 samples with the lowest SiCw content. Therefore, the droplets impacting the 3S5 and 5S5 surfaces lose less kinetic energy than those impacting the 3S2 and 5S2 surfaces, and thus there is a significant rebound height. Combined with the SEM images of 3S5 and 5S5

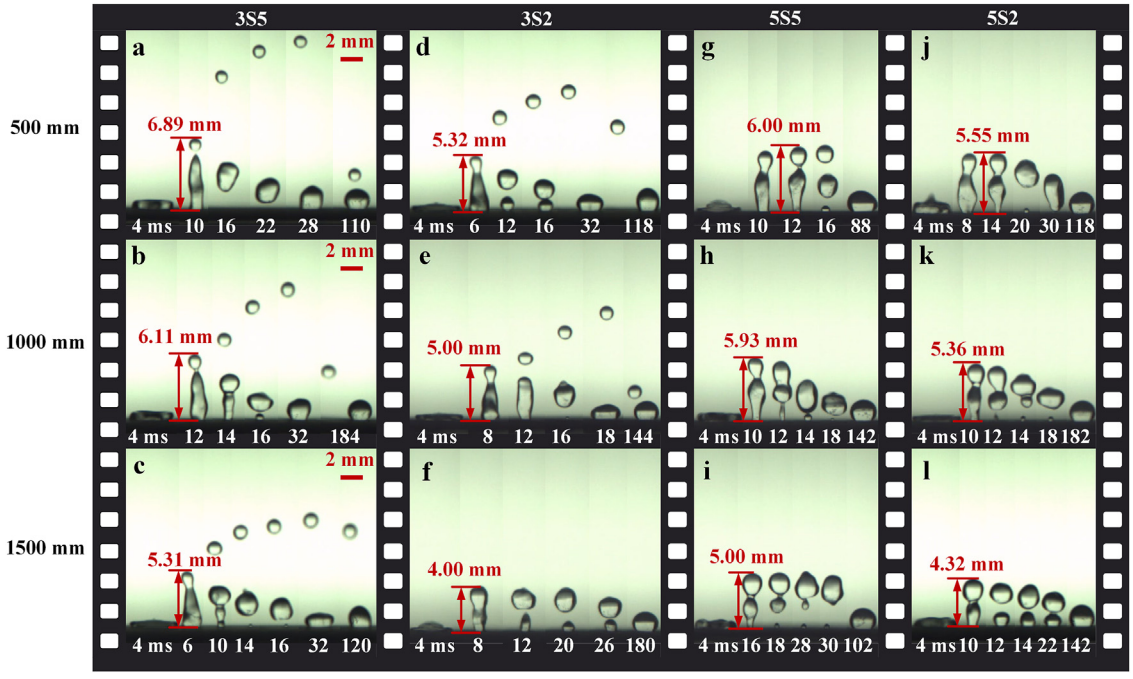

Fig. 8 – Sequential images of droplets impacting onto abraded micropillared PP surfaces molded with (a–f) 3000- and (g–l) 500-mesh sieves coated with 20 and 5 mg/mL SiCw, respectively.

surfaces after wear in Fig. 7, the 3S5 and 5S5 samples molded with sieves coated with 20 mg/mL SiCw maintain their surface structures better after cyclic wear, exhibiting high wear resistance.

A fragmentation phenomenon occurs in the rebound phase of droplets on the micropillared PP surface molded with the 3000-mesh sieve. The droplet broke into two segments consisting of a small droplet emerging from the upper edge of the main droplet due to the pressure difference and a large one with reduced energy due to the dissipation of the surface adhesion work. This is because the droplets coalesce and trap some air during the coalescence process. Air bubbles form in the dynamic droplets, thus causing a pressure difference that leads to the separation of the droplets. The surface adhesion of the two samples, 3S2 and 3S5, was observed after the wear cycle and showed the same trend as the sample molded with the 500-mesh sieve. As the wear distance increases, the growth of adhesion to the sample surface leads to an increase in the hydrophobic surface energy. In addition, the wear experiment destroys the structural integrity of the sample surface, resulting in the loss of the superhydrophobic properties of the sample. The SiCw distributed on the 3S5 and 5S5 surfaces help to maintain their structural integrity of surfaces during friction. Also, the relatively towering rebound height of droplet and low surface adhesion in impact experiments are caused by the SiCw. In fact, although the SiCw have no significant effect on the static wetting behavior of samples, they endow the micropillared PP surfaces with the ability to withstand the penetrating and repel the droplets during the impact test. Obviously, the SiCw are witnessed as the key to wear resistance.

Matthew et al. demonstrated that multi-layered superhydrophobic surface micromorphology combined with nanoparticles can synergistically prevent droplet impact from damaging the superhydrophobic surface [50]. Nanoparticles provide capillary pressure for antiwetting and even lethal stretching sometimes [51]. The microstructure part reduces the contact with the droplet by trapping air. This hinders the development and propagation of pressure during droplet compression. Generally, the microstructure provides durability, and the nanostructure maintains the superhydrophobicity of the material surface. They interact with each other, thus synergistically guaranteeing the structural integrity as well as the superhydrophobicity of the material surface [52]. However, it is found that the microstructure part has provided sufficient superhydrophobicity for the sample, and the high structural wear resistance can be achieved relying on the tiny SiCw, i.e., the nanospiked structures.

3.5. *Antibacterial activities of nanospiked micropillared PP surfaces*

To quantitatively evaluating the antibacterial activities of the nanospiked micropillared PP surfaces, the incubation of the bacterial cultures was performed using a standard plate counting method to count the CFU. Fig. 10 shows the surviving CFU as a function of uncoated flat PP surface, laminated SiCw surface, and micropillared PP surfaces with different SiCw concentrations. For comparison, the flat PP surface and the laminated SiCw surface were used as controls. The CFU of the uncoated flat PP sample is about 1.1×10^6; the laminated SiCw sample has the highest CFU of 1.8×10^7. Obviously, the growth of bacteria is promoted on the SiCw sample. According to this speculation, the bacteria would have been supposed to grow well on nanospiked micropillared PP surfaces, but their CFU values show either an increase or a decrease for the PP samples coated with different SiCw contents. Firstly, the CFU shows a decrease in 3S1 and 5S1 samples exhibiting superhydrophobic properties due to the presence of micropillars without spiked nanoarchitectures. It is speculated that micropillars endow the samples with antibacterial properties, which are improved to varying degrees but not always best compared with the uncoated flat PP sample. To some extent, the reduced adhesion to bacteria is in line with the adhesion trend of nanospiked micropillared PP surfaces.

As the SiCw concentration increases, the CFU values of 3S2, 3S3, 5S2, and 5S3 samples have risen in varying degrees. This is because denser SiCw lead to the proliferation of bacteria.

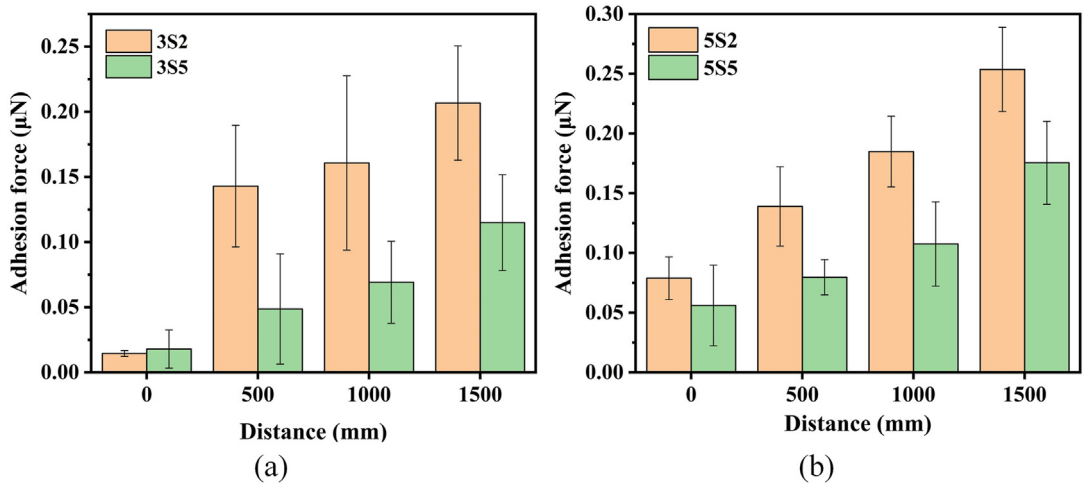

Fig. 9 – Adhesion force of micropillared PP surface molded with (a) 3000- and (b) 500-mesh sieves coated with 5 and 20 mg/mL SiCw before and after wear.

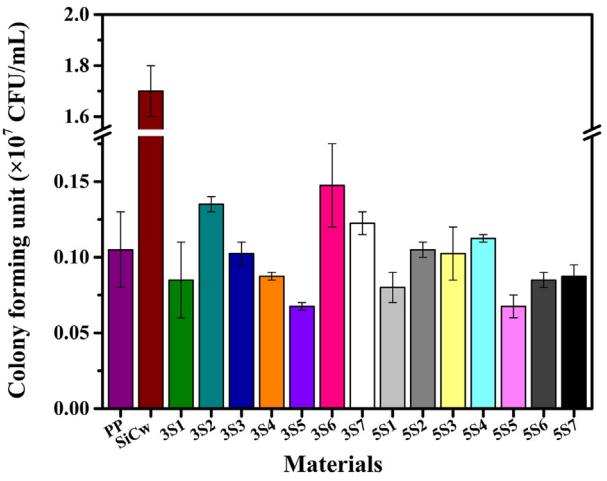

Fig. 10 – Surviving CFU as a function of uncoated flat PP surface, laminated SiCw surface, and micropillared PP surfaces with different SiCw concentrations.

When the SiCw content is ranging from 15 to 25 mg/mL, the 3S4, 3S5, 5S5, and 5S6 samples start to exhibit the ability to inhibit bacterial growth well compared to the uncoated flat PP sample and the laminated SiCw sample. At the same time, the 3S4, 3S5, 5S5, and 5S6 surface exhibit the excellent wear resistance due to the high CA of more than 145° after a certain wear distance. This is because the formation of the standing state for the nanospikes under this SiCw content. Combining the CFU result and the wettability, it can be concluded that 3S5 and 5S5 show the best antibacterial properties by the emergence of SiCw. The antimicrobial efficiency for 3S5 and 5S5 was calculated according to *Eq.* 1, and the corresponding values are 50.0% and 53.8%, respectively. When the SiCw content is ranging from 25 to 30 mg/mL, the CFU of the samples increases again. More specifically, the CFU of the PP samples molded with 3000-mesh sieves is much greater than that with 500-mesh sieves. This is because the small microcavity cannot accommodate overmuch SiCw for the 3000-mesh sieve, and the blocking of the microcavity hinders the formation of well-developed micropillars. It is evident that the SiCw content of 20 mg/mL is the optimized concentration for both robust anti-wetting and anti-bacterial properties.

According to the abovementioned results, 3S5 and 5S5 samples exhibit almost the lower CFU values, and 3S6 and 5S4 samples show an inverse trend due to the relatively high CFU values. To verify the viability of the bacteria on different nanospiked microstructured PP samples, these four samples were further qualitatively analyzed by the fluorescence microscopy and SEM. Fig. 11 shows the fluorescence micrographs of 3S5, 3S6, 5S4, and 5S5 samples. The dye DAPI endows the live bacteria with fluoresce green, while PI enters the damaged cells and causes red fluorescence. Within the field of vision, the number of bacteria on 3S6 sample is more than that on the 3S5 sample. More specifically, most of the bacteria on 3S5 sample are dead because even red fluorescence appears in the merged image (Fig. 11c). Although a small region of fluorescence image also turns light yellow, instead of being induced by the nanospiked microstructure, we believe it was possibly induced by the overlap of the biofilms lacking nutrition and space. Coincidentally, large number of bacteria on 5S4 sample is seen; small number of bacteria on 5S5 sample is seen, and even red fluorescence also appears in the merged image (Fig. 11l). So, not only the number of bacteria on 5S5 sample is much less than that on the 5S4 sample, but also most of bacteria on 5S5 sample are dead. The results evidenced that 3S5 and 5S5 samples possess excellent antibacterial properties.

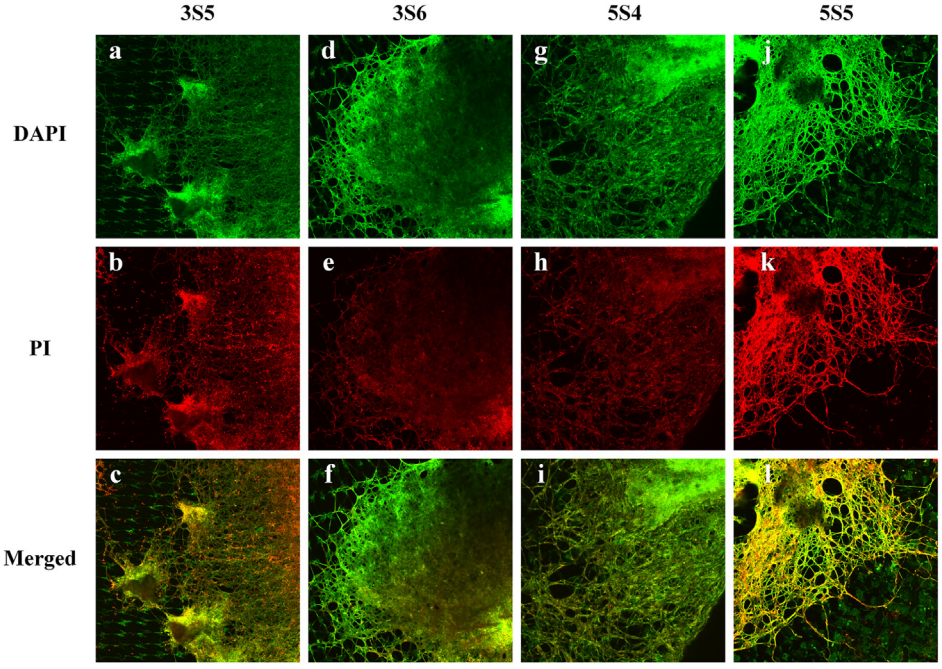

Fig. 11 – Fluorescence microscopy images of *C. albicans* on 3S5, 3S6, 5S4, and 5S5 surfaces.

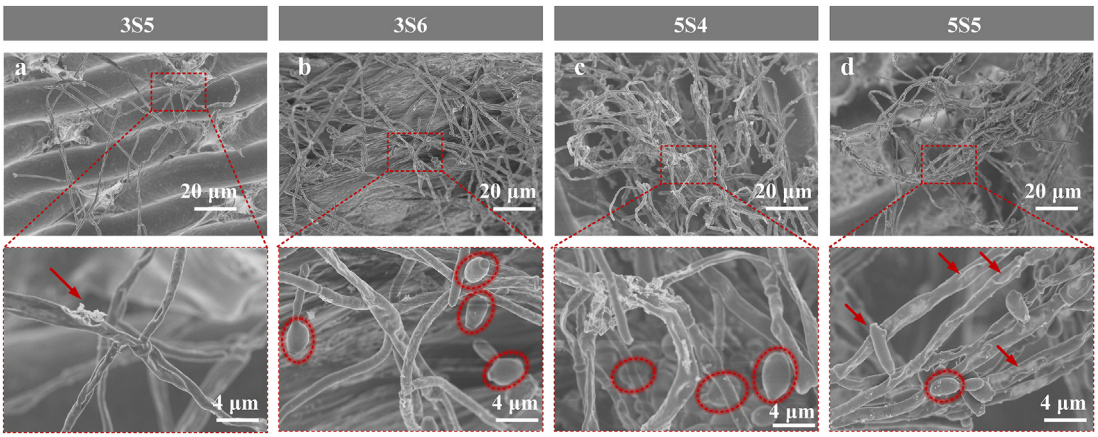

Fig. 12 – SEM images of bacteria on nanospiked micropillared PP surfaces.

These results can also be verified by the SEM magnified images of adhered bacteria cells on these four sample surfaces shown in Fig. 12. On 3S6 and 5S4 surfaces (Fig. 12b and c), the hyphae look sturdy and smooth, and all tangled up, resulting in the formation of aggregated colonies for the bacteria; the budding cells at hyphal tips are abundant, plump, and regularly shaped with a diameter of about 4 μm, indicating that bacteria cells are still full of vitality [53]. Especially, distinct exocytosis phenomena appears at the end of budding cells, indicating that the non-optimized nanospiked micropillared PP surfaces are not sufficient to diminish the proliferation of bacterial cells to the surfaces. On 3S5 and 5S5 sample surfaces (Fig. 12a, d), the hyphae look frail, shriveled, and irregular shaped, indicating that bacteria cells are suffering from a lack of vitality. Especially, distinct cell membrane burst is witnessed, indicating that the optimized nanospiked micropillared PP surfaces can penetrate into the cell membrane by virtue of the nanospiked SiCw and submicron villi, undermine the cell vitality, and lead to the rupturing of cell membranes. Besides, although 5S5 sample surface is dotted with several budding cells, frustrated exocytosis phenomena may occur for the budding cells with a diameter of about 2 μm.

To clarify the mechanism of physical antibacterial activity on the nanospiked micropillared PP surface, the corresponding schematics are depicted in Fig. 13. The optimized nanospiked micropillared PP surfaces contains highly dense high length-diameter ratio SiCw of with a diameter of about 50 nm and length of 10–20 μm embedded in the micropillars, forming fern-like fractal nanospikes. These sharp nanoarchitectures exert a lateral mechanical force acting on the adhered cell membranes on the sample surfaces, resulting in the cell lacking vitality or even the cell death. Further, due to the excellent resistance to water and wear, the nanospiked micropillared PP surfaces decrease proliferation of bacteria

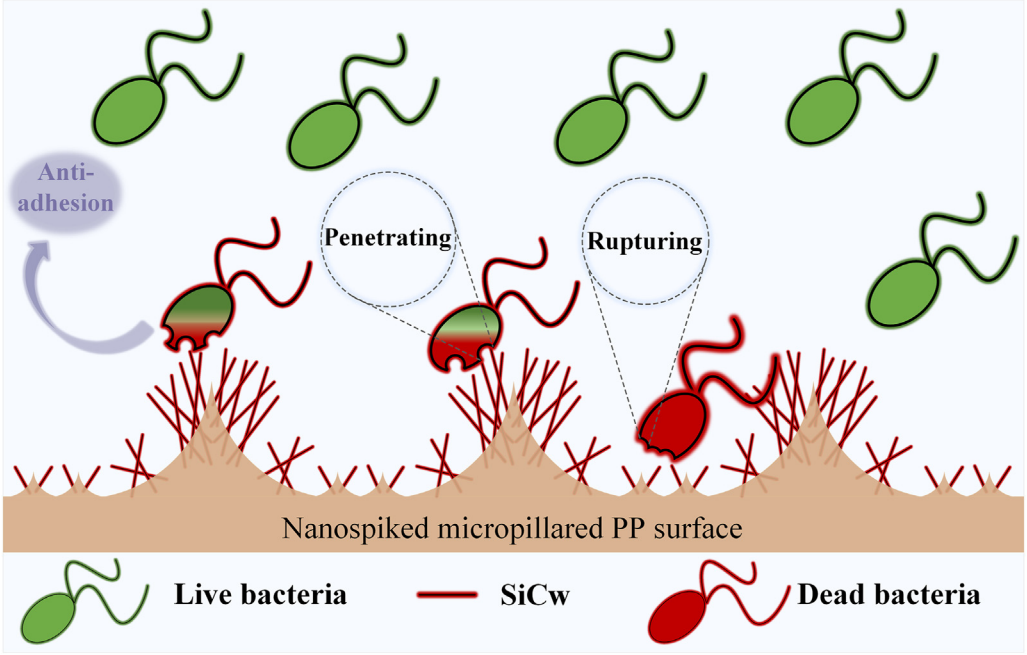

Fig. 13 – Mechanism of physical antibacterial activity for nanospiked micropillared PP surfaces.

Table 1 – Antibacterial activity of micro-/nanostructured surfaces.

Year	Materials	Antibacterial mechanism	Strains	Antibacterial efficiency, %	Manufacturing	Refs.
2023	SiCw/PP	Antibacterial physical structure	*C. albicans*	50 (3S5) 53 (5S5)	Simple, effective, and inexpensive method	this work
2021	Pillars of black titanium (bTi)	Antibacterial physical structure	*S. aureus*	42 ± 7	Reactive ion etching is based on the expensive equipment and has high cost in manufacturing.	[54]
2020	Silicon Nanopillar arrays	Antibacterial physical structure	*P. aeruginosa* *S. aureus*	53 58	Plasma etching has time-consuming and process high cost in manufacturing.	[55]
2021	ZIF@Nd-HA/TiO	Antibacterial agent	*E. coli* *S. aureus*	79.16 83.85	Electrodeposition is limited to conducting substrates and the coating is easily degraded.	[56]
2022	PP-PMPC	Antibacterial agent	*E. coli* *S. aureus*	82.5 82.2	Complex chemical surface modification and toxic substance residues	[57]

and the bio-adhesion to surfaces accompanied by a satisfactory anti-biofouling performance. The nanospikes standing on the pyramid-shaped or cube-shaped micropillars as well as ridge-like architectures acting as the strength against the colonization of *C. albicans* bacteria. Therefore, it can be concluded that the entrapped air pockets in the gaps between the micropillars and between the nanospikes acting as the strength against the colonization of *C. albicans* bacteria.

Further, the good physical antibacterial activities with the advantages of low cost and facile preparation process in this work were compared with recent literature based on superhydrophobic coatings. The corresponding preparation and performance of antimicrobial materials are listed in Table 1. The preferred structures in this work, 3S5 and 5S5, are completely dependent on the physical structure for antibacterial activity with the antibacterial efficiency of 50.0% and 53.8%, respectively. The antibacterial activity in this work is comparable to previous studies on antibacterial physical structure [54,55]. Most importantly, the preparation process used in this work is facile, low-cost, and efficient, and has the potential for industrialization. The antimicrobial efficiency of the physical structure is much lower than that of antimicrobial agent [56,57]. However, the process of complex chemical surface modification is time-consuming. Especially, toxic substance residues are harmful both to animal and human health.

4. Conclusions

By virtue of SiCw-coated sieve templates, two kinds of nanospiked micropillars were constructed on PP surfaces by the micro-compression molding technique. Interestingly, the SiCw were embedded in the surface layer of PP samples and completely exposed in different postures of standing. In fact, the SiCw were designed to form distinctive spiked nanoarchitectures on micropillared PP surfaces by regulating the SiCw concentrations since the microcavities will be blocked by the superfluous SiCw. Also, they enabled the samples to maintain the structural integrity of the surface as well as the highly hydrophobic properties after a certain wear cycle. The results evidenced that 5S5 and 3S5 samples possess excellent antibacterial properties among the samples. That is, the nanospiked micropillared PP surfaces with the optimized SiCw concentration of 20 mg/mL possess the relatively good ability to prevent *C. albicans* bacterial adhesion as well as growth or even penetrate into bacteria cells by virtue of the nanospiked micropillars. The nanospikes standing on the pyramid-shaped or cube-shaped micropillars as well as ridge-like architectures acting as the strength against the colonization of *C. albicans* bacteria.

CRediT authorship contribution statement

Jindi Lai: Investigation, Methodology, Software, Writing – original draft, Writing – review & editing. **Anfu Chen:** Investigation, Methodology, Writing – review & editing, Supervision, Funding acquisition. **Jing Li:** Software. **Yameng Pei:** Data curation. **Seyed Ataollah Naghavi:** Validation. **Caihong Lei:** Supervision. **Chaozong Liu:** Supervision. **Lijia Huang:** Data curation, Supervision, Writing – review & editing.

Declaration of competing interest

The authors declare that they have no known competing financial interests or personal relationships that could have appeared to influence the work reported in this paper.

Acknowledgments

This work was supported by the National Natural Science Foundation of China (Grant nos. 52003057 and 82201039), Foshan Science and Technology Innovation Project (Grant no. FS0AA-KJ919-4402-0145), the Natural Science Foundation of Guangdong Province, China (Grant no. 2020A1515110064), MRC - UCL Therapeutic Acceleration Support (TAS) Fund (project no. 564022), NIHR UCLH BRC - UCL Therapeutic Acceleration Support (TAS) Fund (project no. 564021), and Engineering and Physical Sciences Research Council via DTP CASE Programme (Grant no. EP/T517793/1). We Would like to thank

Mr. Kai Yan at Analysis and Test Center of Guangdong University of Technology for his assistance with the surface tension apparatus analysis.

Appendix A. Supplementary data

Supplementary data to this article can be found online at https://doi.org/10.1016/j.jmrt.2023.01.069.

REFERENCES

[1] Kembel SW, O'Connor TK, Arnold HK, Hubbell SP, Wright SJ, Green JL. Relationships between phyllosphere bacterial communities and plant functional traits in a neotropical forest. Proc Natl Acad Sci USA 2014;111:13715–20.

[2] Kraft NJB, Godoy O, Levine JM. Plant functional traits and the multidimensional nature of species coexistence. Proc Natl Acad Sci USA 2015;112:797–802.

[3] Barton KE. Tougher and thornier: general patterns in the induction of physical defence traits. Funct Ecol 2016;30:181–7.

[4] Hanley ME, Lamont BB, Fairbanks MM, Rafferty CM. Plant structural traits and their role in anti-herbivore defence. Plant Ecol. Evol. Syst. 2007;8:157–78.

[5] Ivanova EP, Hasan J, Webb HK, Truong VK, Watson GS, Watson JA, et al. Natural bactericidal surfaces: mechanical rupture of pseudomonas aeruginosa cells by cicada wings. Small 2012;8:2489–94.

[6] Jiang RJ, Hao WL, Song LJ, Tian LM, Fan Y, Zhao J, et al. Lotus-leaf-inspired hierarchical structured surface with non-fouling and mechanical bactericidal performances. Chem Eng J 2020;398:125609.

[7] Watson GS, Green DW, Cribb BW, Brown CL, Meritt CR, Tobin MJ, et al. Insect analogue to the lotus leaf: a planthopper wing membrane incorporating a low-adhesion, nonwetting, superhydrophobic, bactericidal, and biocompatible surface. ACS Appl Mater Interfaces 2017;9:24381–92.

[8] Linklater DP, Baulin VA, Juodkazis S, Crawford RJ, Stoodley P, Ivanova EP. Mechano-bactericidal actions of nanostructured surfaces. Nat Rev Microbiol 2021;19:8–22.

[9] Kelleher SM, Habimana O, Lawler J, O'Reilly B, Daniels S, Casey E, et al. Cicada wing surface topography: an investigation into the bactericidal properties of nanostructural features. ACS Appl Mater Interfaces 2016;8:14966–74.

[10] Shang MW, Samuel MS, Biswas S, Niu JJ. dual-layered SiO_2 nanoparticles and epoxy polymers for self-cleaning coatings on ceramic glaze. ACS Appl Nano Mater 2022;5:15934–41.

[11] Zhuo YZ, Chen JH, Xiao SB, Li T, Wang F, He JY, et al. Gels as emerging anti-icing materials: a mini review. Mater Horiz 2021;8:3266–80.

[12] Park C, Kim T, Kim YI, Kim YI, Lee MW, An S, et al. Supersonically sprayed transparent flexible multifunctional composites for self-cleaning, anti-icing, anti-fogging, and anti-bacterial applications. Compos B Eng 2021;222:109070.

[13] Zhu YJ, Sun FL, Qian HJ, Wang HY, Mu LW, Zhu JH. A biomimetic spherical cactus superhydrophobic coating with durable and multiple anti-corrosion effects. Chem Eng J 2018;338:670–9.

[14] Hu JT, Lin J, Zhang YY, Lin ZK, Qiao ZW, Liu ZL, et al. A new anti-biofilm strategy of enabling arbitrary surfaces of materials and devices with robust bacterial anti-adhesion via a spraying modified microsphere method. J Mater Chem 2020;7:26039–52.

[15] He G, Yang CD, Feng JM, Wu JM, Zhou LF, Wen R, et al. Hierarchical spiky microstraws-integrated microfluidic device for efficient capture and in situ manipulation of cancer cells. Adv Funct Mater 2019;29:1806484.

[16] Gao AL, Zhao YQ, Yang Q, Fu YY, Xue LX. Facile preparation of patterned petal-like PLA surfaces with tunable water micro-droplet adhesion properties based on stereo-complex co-crystallization from non-solvent induced phase separation processes. J Mater Chem 2016;4:12058–64.

[17] Zhong H, Zhu ZR, Lin J, Cheung CF, Lu VL, Yan F, et al. Reusable and recyclable graphene masks with outstanding superhydrophobic and photothermal performances. ACS Nano 2020;14:6213–21.

[18] Li J, Wang WJ, Mei XS, Pan AF. Designable ultratransparent and superhydrophobic surface of embedded artificial compound eye with extremely low adhesion. ACS Appl Mater Interfaces 2020;12:53557–67.

[19] Li J, Wang WJ, Zhu RX, Huang YX. Superhydrophobic artificial compound eye with high transparency. ACS Appl Mater Interfaces 2021;13:35026–37.

[20] Zhang YM, Chen XS, Luo CJ, Gu JC, Li MR, Chao M, et al. Column-to-beam structure house inspired MXene-based integrated membrane with stable interlayer spacing for water purification. Adv Funct Mater 2022;32:2111660.

[21] Niu HS, Zhang HY, Yue WJ, Gao S, Kan H, Zhang CW, et al. Micro-nano processing of active layers in flexible tactile sensors via template methods: a review. Small 2021;17:2100804.

[22] Wang F, Ren F, Ma D, Mu P, Wei HJ, Xiao CH, et al. Particle and nanofiber shaped conjugated microporous polymers bearing hydantoin-substitution with high antibacterial activity for water cleanness. J Mater Chem 2018;6:266–74.

[23] Wang YM, Wang F, Zhang H, Yu B, Cong HL, Shen YQ. Antibacterial material surfaces/interfaces for biomedical applications. Appl Mater Today 2021;25:101192.

[24] Linklater DP, De Volder M, Baulin VA, Werner M, Jessl S, Golozar M, et al. High aspect ratio nanostructures kill bacteria via storage and release of mechanical energy. ACS Nano 2018;12:6657–67.

[25] Lin N, Berton P, Moraes C, Rogers RD, Tufenkji N. Nanodarts, nanoblades, and nanospikes: mechano-bactericidal nanostructures and where to find them. Adv Colloid Interface Sci 2018;252:55–68.

[26] Wan T, Wang B, Han Q, Chen JS, Li BC, Wei SC. A review of superhydrophobic shape-memory polymers: preparation, activation, and applications. Appl Mater Today 2022;29:101665.

[27] Moghadam SG, Parsimehr H, Ehsani A. Multifunctional superhydrophobic surfaces. Adv Colloid Interface Sci 2021;290:102397.

[28] Zhang CJ, Liang FH, Zhang W, Liu H, Ge MZ, Zhang YY, et al. Constructing mechanochemical durable and self-healing superhydrophobic surfaces. ACS Omega 2020;5:986–94.

[29] Wang P, Li CY, Zhang D. Recent advances in chemical durability and mechanical stability of superhydrophobic materials: multi-strategy design and strengthening. J Mater Sci Technol 2022;129:40–69.

[30] Cao CY, Yi B, Zhang JQ, Hou CS, Wang ZY, Lu G, et al. Sprayable superhydrophobic coating with high processibility and rapid damage-healing nature. Chem Eng J 2020;392:124834.

[31] Quan YY, Chen Z, Lai YK, Huang ZS, Li HQ. Recent advances in fabricating durable superhydrophobic surfaces: a review in the aspects of structures and materials. Mater Chem Front 2021;5:1655–82.

[32] Arango-Ospina M, Xie FT, Juan IG, Riedel R, Ionescu E, Boccaccini AR. Review: silicon oxycarbide based materials for biomedical applications. Appl Mater Today 2020;18:100482.
[33] Roy A, Chatterjee K. Bactericidal anisotropic nanostructures on titanium fabricated by maskless dry etching. ACS Appl Nano Mater 2022;5:4447–61.
[34] Arias SL, Devorkin J, Spear JC, Civantos A, Allain JP. Bacterial envelope damage inflicted by bioinspired nanostructures grown in a hydrogel. ACS Appl Bio Mater 2020;3:7974–88.
[35] Wong WSY, Stachurski ZH, Nisbet DR, Tricoli A. Ultra-durable and transparent self-cleaning surfaces by large-scale self-assembly of hierarchical interpenetrated polymer networks. ACS Appl Mater Interfaces 2016;8:13615–23.
[36] Li FR, Wang ZR, Huang SC, Pan YL, Zhao XZ. Flexible, durable, and unconditioned superoleophobic/superhydrophilic surfaces for controllable transport and oil-water separation. Adv Funct Mater 2018;28:1706867.
[37] Hwang GB, Patir A, Page K, Lu Y, Allan E, Parkin IP. Buoyancy increase and drag-reduction through a simple superhydrophobic coating. Nanoscale 2017;9:7588–94.
[38] Golovin K, Boban M, Mabry JM, Tuteja A. Designing self-healing superhydrophobic surfaces with exceptional mechanical durability. ACS Appl Mater Interfaces 2017;9:11212–23.
[39] Tripathy A, Sen P, Su B, Briscoe WH. Natural and bioinspired nanostructured bactericidal surfaces. Adv Colloid Interface Sci 2017;248:85–104.
[40] Maghsoudi K, Vazirinasab E, Momen G, Jafari R. Icephobicity and durability assessment of superhydrophobic surfaces: the role of surface roughness and the ice adhesion measurement technique. J Mater Process Technol 2021;288:116883.
[41] Chen AF, Lai JD, Li MK, Fang CK, Qin GF, Ding S, et al. Long-lived T-shaped micropillars with submicron-villi on PP/POE surfaces with grinding-enhanced water repellency fabricated via hot compression molding. J Phys Chem B 2021;125:7290–8.
[42] Tang YN, Sun H, Shang YX, Zeng S, Qin Z, Yin SY, et al. Spiky nanohybrids of titanium dioxide/gold nanoparticles for enhanced photocatalytic degradation and anti-bacterial property. J Colloid Interface Sci 2019;535:516–23.
[43] Bandara HMHN, Yau JYY, Watt RM, Jin LJ, Samaranayake LP. Pseudomonas aeruginosa inhibits in-vitro candida biofilm development. BMC Microbiol 2010;10:125.
[44] Comer JJ. A study of contrast bands in β-SiC whiskers. Mater Res Bull 1969;4:279–87.
[45] Zhang X, Mo JL, Si YF, Guo ZG. How does substrate roughness affect the service life of a superhydrophobic coating? Appl Surf Sci 2018;441:491–9.
[46] Zhang YM, Xing QS, Chen AF, Li MK, Qin GF, Zhang JJ, et al. Turning hierarchically micro-/nanostructured polypropylene surfaces robustly superhydrophobic via tailoring contact line density of mushroom-shaped nanostructure. Chem Eng Sci 2022;262:118027.
[47] Choi W, Tuteja A, Mabry JM, Cohen RE, McKinley GH. A modified Cassie–Baxter relationship to explain contact angle hysteresis and anisotropy on non-wetting textured surfaces. J Colloid Interface Sci 2009;339:208–16.
[48] Zhang YM, Liu ZB, Chen AF, Wang QK, Zhang JJ, Zhao C, et al. Fabrication of micro-/submicro-/nanostructured polypropylene/graphene superhydrophobic surfaces with extreme dynamic pressure resistance assisted by single hierarchically porous anodic aluminum oxide template. J Phys Chem C 2020;124:6197–205.
[49] Xia ZY, Zhao Y, Yang Z, Yang CJ, Li LA, Wang SB, et al. The simulation of droplet impact on the super-hydrophobic surface with micro-pillar arrays fabricated by laser irradiation and silanization processes. Colloid Surf. A-Physicochem. Eng. Asp. 2021;612:125966.
[50] McCarthy M, Gerasopoulos K, Enright R, Culver JN, Ghodssi R, Wang EN. Biotemplated hierarchical surfaces and the role of dual length scales on the repellency of impacting droplets. Appl Phys Lett 2012;100:263701.
[51] Linklater DP, Baulin VA, Le Guével X, Fleury JB, Hanssen E, Nguyen THP, et al. Antibacterial action of nanoparticles by lethal stretching of bacterial cell membranes. Adv Mater 2020;32:2005679.
[52] Wang DH, Sun QQ, Hokkanen MJ, Zhang CL, Lin FY, Liu Q, et al. Design of robust superhydrophobic surfaces. Nature 2020;582:55–9.
[53] Agarwalla SV, Ellepola K, Silikas N, Castro Neto AH, Seneviratne CJ, Rosa V. Persistent inhibition of candida albicans biofilm and hyphae growth on titanium by graphene nanocoating. Dent Mater 2021;37:370–7.
[54] Modaresifar K, Ganjian M, Angeloni L, Minneboo M, Ghatkesar MK, hagedoorn PL, et al. On the use of black Ti as a bone substituting biomaterial: behind the scenes of dual-functionality. Small 2021;17:2100706.
[55] Ivanova EP, Linklater DP, Werner M, Baulin VA, Xu XM, Vrancken N, et al. The multi-faceted mechano-bactericidal mechanism of nanostructured surfaces. Proc Natl Acad Sci USA 2020;117:12598–605.
[56] Zhang ZQ, Zhang Y, Liu Y, Zhang SQ, Yao KD, Sun YQ, et al. Electro-deposition of Nd3+-doped metal-organic frameworks on titanium dioxide nanotube array coated by hydroxyapatite for anti-microbial and anticorrosive implant. Ionics 2021;27:2707–15.
[57] Jiang L, Qin N, Gu S, Zhu WC, Wang CH, Chen YS. Rational design of dual-functional surfaces on polypropylene with antifouling and antibacterial performances via a micropatterning strategy. J Math Chem B 2022;10:3759–69.